Different mechanisms involved in apoptosis following exposure to benzo[a]pyrene in F258 and Hepa1c1c7 cells.

Jørn A. Holme, Morgane Gorria, Volker M. Arlt, Steinar Ovrebø, Anita Solhaug, Xavier Tekpli, Nina E Landvik, Laurence Huc, Olivier Fardel, Dominique Lagadic-Gossmann

Available online at www.sciencedirect.com
ScienceDirect
Chemico-Biological Interactions 167 (2007) 41–55
Chemico-Biological Interactions
www.elsevier.com/locate/chembioint

Different mechanisms involved in apoptosis following exposure to benzo[*a*]pyrene in F258 and Hepa1c1c7 cells

Jørn A. Holme [a,*], Morgane Gorria [b], Volker M. Arlt [c], Steinar Øvrebø [d], Anita Solhaug [a], Xavier Tekpli [b], Nina E. Landvik [a], Laurence Huc [b], Olivier Fardel [b], Dominique Lagadic-Gossmann [b]

[a] *Division of Environmental Medicine, Norwegian Institute of Public Health, P.O. Box 4404 Nydalen, N-0403 Oslo, Norway*
[b] *Inserm U620, Université Rennes 1, IFR 140, 2 av Pr. Léon Bernard, 35043 Rennes Cédex, France*
[c] *Section of Molecular Carcinogenesis, Institute of Cancer Research, Sutton, Surrey SM2 5NG, United Kingdom*
[d] *Section for Toxicology, National Institute of Occupational Health, P.O. Box 8149 Dep., N-0033 Oslo, Norway*

Received 27 October 2006; received in revised form 21 December 2006; accepted 8 January 2007
Available online 17 January 2007

Abstract

The present study compares and elucidates possible mechanisms why B[*a*]P induces different cell signals and triggers apparently different apoptotic pathways in two rather similar cell lines (hepatic epithelial cells of rodents). The rate and maximal capacity of metabolic activation, as measured by the formation of B[*a*]P-tetrols and B[*a*]P-DNA adducts, was much higher in mouse hepatoma Hepa1c1c7 cells than in rat liver epithelial F258 cells due to a higher induced level of cyp1a1. B[*a*]P increased intracellular pH in both cell lines, but this change modulated the apoptotic process only in F258 cells. In Hepa1c1c7 cells reactive oxygen species (ROS) production appeared to be a consequence of toxicity, unlike F258 cells in which it was an initial event. The increased mitochondrial membrane potential found in F258 cells was not observed in Hepa1c1c7 cells. Surprisingly, F258 cells cultured at low cell density were somewhat more sensitive to low (50 nM) B[*a*]P concentrations than Hepa1c1c7 cells. This could be explained partly by metabolic differences at low B[*a*]P concentrations. In contrast to the Hepa1c1c7 model, no activation of cell survival signals including p-Akt, p-ERK1/2 and no clear inactivation of pro-apoptotic Bad was observed in the F258 model following exposure to B[*a*]P. Another important difference between the two cell lines was related to the role of Bax and cytochrome *c*. In Hepa1c1c7 cells, B[*a*]P exposure resulted in a "classical" translocation of Bax to the mitochondria and release of cytochrome *c*, whereas in F258 cells no intracellular translocation of these two proteins was seen. These results suggest that the rate of metabolism of B[*a*]P and type of reactive metabolites formed influence the resulting balance of pro-apoptotic and

Abbreviations: α-NF, α-naphthoflavone; AhR, aryl hydrocarbon receptor; B[*a*]P, benzo[*a*]pyrene; B[*a*]P-3-OH, (±)-3-hydroxy-benzo[*a*]pyrene; B[*a*]P-9-OH, (±)-9-hydroxy-benzo[*a*]pyrene; B[*a*]P-4,5-DHD, (±)-benzo[*a*]pyrene-*trans*-4,5-dihydrodiol; B[*a*]P-7,8-DHD, (±)-benzo[*a*]pyrene-*trans*-7,8-dihydrodiol; B[*a*]P-9,10-DHD, (±)-benzo[*a*]pyrene-*trans*-9,10-dihydrodiol; B[*a*]P-tetrol-I-1, (±)-benzo[*a*]pyrene-r-7,t-8,9,c-10-tetrahydrotetrol; B[*a*]P-tetrol-I-2, (±)-benzo[*a*]pyrene-r-7,t-8,9,10-tetrahydrotetrol; B[*a*]P-tetrol-II-1, (±)-benzo[*a*]pyrene-r-7,t-8,c-9,t-10-tetrahydrotetrol; B[*a*]P-tetrol-II-2, (±)-benzo[*a*]pyrene-r-7,t-8,c-9,10-tetrahydrotetrol; BPDE-I, r-7,t-8-dihydrodiol-t-9,10-oxy-7,8,9,10-tetrahydrobenzo[*a*]pyrene; BPDE-II, r-7,t-8-dihydrodiol-c-9,10-oxy-7,8,9,10-tetrahydrobenzo[*a*]pyrene; cyp, cytochrome P450; DMSO, dimethyl sulphoxide; ERK, extracellular signal-related kinase; FCS, foetal calf serum; pH_i, intracellular pH; JNK, c-jun N-terminal kinase; MAPK, mitogen-activated kinases; PAHs, polycyclic aromatic hydrocarbons; NHE1, Na^+/H^+ exchanger 1; PI, propidium iodide; PKA, protein kinase A; ROS, reactive oxygen species

* Corresponding author. Tel.: +47 22 04 22 47; fax: +47 22 04 26 86.
E-mail address: jorn.holme@fhi.no (J.A. Holme).

doi:10.1016/j.cbi.2007.01.008

anti-apoptotic cell signaling, and hence the mechanisms involved in cell death and the chances of more permanent genetic damage.

Keywords: Benzo[*a*]pyrene; Cell signaling; DNA adducts; Metabolism; Apoptosis

1. Introduction

Polycyclic aromatic hydrocarbons (PAHs) are major environmental and occupational pollutants formed during incomplete combustion (burning) of organic material such as gasoline, diesel fuel, coal, oil, tobacco and during the grilling, barbecuing or smoking of food [1]. These substances are therefore found in air, water, soil and food, and based on epidemiological and animal studies many of them are considered to be carcinogenic [2].

Several PAHs, including benzo[*a*]pyrene B[*a*]P, bind and activate a ligand-dependent transcription factor termed the aryl hydrocarbon receptor (AhR) [3]. Ligand-activated AhR complexes can interact with specific promoter elements called AhR-mediated aromatic hydrocarbon response elements (AHRE), which are present in the 5′-region of a subset of cellular genes including *cyp1a1*, *cyp1a2* and *cyp1b1*. In this way, the PAHs promote their own metabolism. In general, most of the parent compounds are detoxified. However, PAHs may also damage the cells by being metabolized to reactive electrophilic species that covalently bind to cellular macromolecules including DNA. Presently, the most mutagenic and tumorigenic diol-epoxides are considered to be those formed at the bay region of PAHs. These diol-epoxides are partly protected from hydrolysis by epoxide hydrolase due to steric hindrance. The reactive electrophilic B[*a*]P metabolite r-7,t-8-dihydrodiol-t-9,10-oxy-7,8,9,10-tetrahydrobenzo[*a*]-pyrene (BPDE-I; BPDE) binds to DNA and generates bulky DNA adducts, primarily at deoxyguanosine. Many of the DNA adducts formed are quite stable, and have been found in tissues of exposed experimental animals as well as in humans [4]. While the ubiquity of these adducts suggests a role in the carcinogenesis process due to the fact that many of them result in mutagenic lesions, there are also other well documented mechanisms by which B[*a*]P can damage DNA, cause mutations, apoptosis and inflammation. B[*a*]P can be enzymatically directly converted into a radical cation forming unstable DNA adducts [5]. Furthermore, (±)-B[*a*]P-*trans*-7,8-dihydrodiol (B[*a*]P-7,8-DHD) is a substrate for dihydrodiol dehydrogenase, resulting in a catechol. The catechols may undergo one electron redox cycling forming semiquinone radicals and quinones. In addition to be DNA reactive themselves, these B[*a*]P metabolites may result in the formation of reactive oxygen species (ROS) including superoxide ($O_2^{\bullet -}$), hydroxyl radical ($OH^{\bullet}$) and hydrogen peroxide (H_2O_2) [6]. These reactive species may also lead to DNA damage that may cause apoptosis, as well as be expressed as mutations by misreplication or misrepair of the DNA damage.

Qualitative as well as quantitative characteristics of DNA damage determines its potential to be properly repaired, cause mutations or end in apoptosis [7–9]. Formation of DNA damage is considered to be an important part of PAH-induced cancer development. However, the fact that cancer cells often are characterized by mutations in the tumor suppressor gene p53 not only suggests an important role of DNA damage, but also points to an important role of cell death in the process since the mutation most often results in defects in their apoptotic machinery [10,11]. Apoptosis induced by genotoxic carcinogens such as PAHs thus seems to have an important role in cancer development. In general, apoptosis of cells exposed to PAHs is considered to function anti-carcinogenic since cells with extensive DNA damage will be removed. On the other hand it is possible that removal of these cells may give survival and proliferating signals to surrounding cells with less DNA damage, increasing their probability of having mutations. Furthermore, due to defects in the apoptotic machinery found in many preneoplasic cells, continuous exposure to carcinogens may preferentially reduce cell growth (reduced proliferation and increased apoptosis) in normal cells. This may cause a selection of these more progressive cancer cells which may be an important part of neoplastic promotion and progression.

Thus, in separate studies we have studied mechanisms involved in B[*a*]P-induced apoptosis using different cell models. The studies suggest that B[*a*]P may induces apoptosis through different mechanisms. In the Hepa1c1c7 model, B[*a*]P-induced apoptosis develops over a period of 24 h [12–14]. The main apoptotic steps have been found to be dependent on cyp1a1 induction and formation of reactive BPDE probably resulting in DNA damage which is detected by a ATM/DNA-PK resulting in activation and translocation of p53. Further important downstream processes include activation of caspase-3 resulting in cleavage of PARP and DNA-

fragmentation. Interestingly, apoptotic Bad is inactivated and cell survival signals Akt and ERK1/2 are activated. Studies using this model have suggested that the relative proportion of the different cell signaling pathways triggered by induced-DNA damage will to a large degree determine if the compound will be mutagenic or mostly give cytotoxic effects.

Using the F258 model, B[*a*]P-induced apoptosis develops over a period of 48–72 h [15,16]. Experiments have revealed that metabolism of B[*a*]P, through enhancing the production of ROS, causes activation of a Na^+/H^+ exchanger 1 (NHE1) resulting in increased intracellular pH (pH_i). This alkalinization combined with an activation of p53 will cause a mitochondrial dysfunction resulting in superoxide anion formation and a late acidification. This favors both activation of executive caspase-3 and recruitment of the pH_i-sensitive LEI/L-DNase II, whereas cytochrome *c* does not seem to be involved in this B[*a*]P-induced apoptotic cascade. Thus, various epigenetic changes as well as possibly effects on the DNA and cell divisions may be needed in this apoptotic process.

In order to be able to make more general implications of these findings, the present study more directly compares and throws more light on possible mechanisms why B[*a*]P induces different cell signals and apparently triggers two clearly distinct apoptotic pathways in two rather similar cell lines (hepatic epithelial cells of rodents).

2. Materials and methods

2.1. Chemicals

Benzo[*a*]pyrene (B[*a*]P), Triton X-100, Ponceau S, dimethyl sulphoxide (DMSO), propidium iodide (PI), Nonidet P-40, phenylmethylsulphonyl fluoride (PMSF), Hoechst 33258, Hoechst 33342, were obtained from Sigma–Aldrich Chemical Company (St. Louis, MO, USA). May-Grunwald and Giemsa was purchased from Merck and Co. Inc. (New Jersey, USA). Pepstatin A was from Calbiochem (Cambridge, MA, CA, USA). Leupeptin from Amersham Biosciences (Uppsala, Sweden) and Bio-Rad DC protein assay from Bio-Rad Laboratories Inc. (Hercules, CA, USA). MEM alpha medium with L-glutamine, without ribonucleosides and deoxyribonucleosides, Williams' E Medium without L-glutamine, foetal calf serum (FCS), penicillin/streptomycin, L-glutamine and gentamycin were from Gibco BRL (Paisley, Scotland, UK). All other chemicals were purchased from commercial sources and were of analytical grade. Cariporide, an inhibitor of the Na^+/H^+ exchange isoform 1, was a kind gift from Aventis (Frankfurt, Germany). Enzymes and chemicals for the ^{32}P-postlabelling assay were obtained from commercial sources as before [17].

2.2. Chemicals for high performance liquid chromatography (HPLC) analyses

(±)-Benzo[*a*]pyrene-r-7,t-8,9,c-10-tetrahydrotetrol (B[*a*]P-tetrol-I-1), (±)-benzo[*a*]pyrene-r-7,t-8,9,10-tetrahydrotetrol (B[*a*]P-tetrol-I-2), (±)-benzo[*a*]pyrene-r-7,t-8,c-9,t-10-tetrahydrotetrol (B[*a*]P-tetrol-II-1), (±)-benzo[*a*]pyrene-r-7,t-8,c-9,10-tetrahydrotetrol (B[*a*]P-tetrol-II-2), B[*a*]P-7,8-DHD, B[*a*]P-4,5-DHD, (±)-benzo[*a*]pyrene-*trans*-9,10-dihydrodiol (B[*a*]P-9,10-DHD) and (±)-3-hydroxy-benzo[*a*]pyrene (B[*a*]P-3OH) were purchased from the National Cancer Institute, Chemical Carcinogen Repository (Midwest Research Institute, Kansas City, MO, USA). Methanol was from Lab-Scan (Stillorgan, Ireland).

2.3. Antibodies

Antibodies against Bcl-x_L, Bad, phospho-Bad (Ser112), phospho-ERK, Akt and phospho-Akt were obtained from Cell Signaling (Beverly, MA, USA); ERK1/2 and cyp1a1 from Santa Cruz Biotechnology Inc. (CA, USA) and cyp1b1 from Alpha Diagnostics (San Antonio, USA). As secondary antibodies horseradish peroxidase-conjugated goat anti-rabbit (Sigma Chemical Company, St. Louis, MO, USA), horseradish peroxidase-conjugated rabbit anti-goat or rabbit anti-mouse IgG from Dako (Glostrup, Denmark) was applied. Rabbit polyclonal anti-Bax and anti-cytochrome *c* antibodies were purchased from Santa Cruz Biotechnology (Tebu-bio SA, Le Perray en Yvelynes, France). Mouse monoclonal anti-COX IV (clone 1D6) was purchased from Molecular Probes (Eugene, OR, USA). Fluorescein isothiocyanate (FITC)-conjugated anti-mouse IgG and tetrarhodamine isothiocyanate (TRITC)-conjugated anti-rabbit IgG were purchased from Sigma Chemicals Co. (St. Louis, MO, USA).

2.4. Cell culture

The mouse hepatoma Hepa1c1c7 cell line was purchased from European Collection of Cell Culture (ECACC). Maintenance of cells was done according to ECACC's guidelines and they were grown in alpha MEM medium with 2 mM L-glutamine, without ribonucleotides and deoxyribonucleotides. Heat-inactivated foetal calf serum (FCS, 10%) and 0.1 mg/mL of gentamycin were added to the medium. Cells were incubated

in 5% CO_2 at 37 °C and passaged every week as previously described [13]. For treatment cells were seeded the day before exposure in dishes or trays at a concentration of either 2.5×10^3 cells/cm^2 (low cell density, reaching confluence at 72–96 h) or 90×10^3 cells/cm^2 (high cell density, reaching confluence during the first 24 h) or 20×10^3 cells/cm^2 (DNA adduct analysis). Fresh medium was added before exposure. Inhibitors were pre-incubated for 1–2 h before adding B[*a*]P in DMSO (not exceeding ≤0.5%).

The F258 rat liver epithelial cell line was cultured in Williams' E medium supplemented with 10% FCS, 2 mM L-glutamine, 5 units/mL penicillin and 0.5 mg/mL streptomycin at 37 °C under a 5% CO_2 atmosphere as previously described [18]. Cells were passaged every week using 0.1% trypsin–EDTA solution. F258 cells, growing in exponential phase, were treated 24 h following seeding (same conditions as for Hepa1c1c7 cells) with B[*a*]P and/or the different inhibitors tested (applied to cells 2 h prior to PAH exposure) for various treatment times.

2.5. Detection of apoptosis

2.5.1. Fluorescence microscopy

Plasma membrane damage, changes in nuclear morphology associated with apoptosis and necrosis was determined after trypsination and staining of the cells with Hoechst 33342 and PI as previously described [13]. At least 300 cells were counted per slide.

2.5.2. Flow cytometry

After treatment cells were trypsinated and prepared for flow cytometry as previously described [19]. In short, the DNA of cells was stained with Hoechst 33258 and fluorescence was measured using an Argus 100 Flow cytometer (Skatron, Lier, Norway). Different cell phases as well as apoptotic cells/bodies were distinguished on the basis of their DNA content (Hoechst fluorescence) and cell size (forward light scatter). The percentages of cells in different phases of the cell cycle as well as apoptotic cells were estimated from DNA histogram using the Multicycle Program (Phoenix Flow System, San Diego, CA, USA). Apoptotic index was determined as the percentage of signals between the G_1 peak and the channel positioned at 20% of the G_1 peak (sub-G_1 population).

2.6. HPLC analysis

Concentrations of the B[*a*]P standard metabolites were determined by UV absorbance of the compounds dissolved in ethanol and employing extinction coefficient from the National Cancer Institute, Chemical Carcinogen Repository (Midwest Research Institute, Kansas City, MO, USA).

Metabolites excreted into the medium were analyzed. Cell culture supernatants were deconjugated with an enzyme mix of β-glucoronidase and arylsulphatase (Boehringer, Mannheim, Germany) and applied to primed Sep-pak C_{18} (Waters, Milford, MA, USA) as previously described [14]. The relative amount and metabolic profile found was similar to that when combined cell and media extracts were analyzed (data not shown). The Sep-pak eluate was evaporated to dryness at 45 °C with N_2 gas and dissolved in 100 μL methanol. Two to 40 μL were injected in the HPLC for quantitative analysis. HPLC analysis was performed on a Zorbax XDB-C_8 (4.6 mm × 150 mm column, 5 μm, Agilent Technologies) with a flow of 1.0 mL/min with a Agilent 1100 HPLC Systems (Agilent Technologies, Waldbronn, Germany) equipped with Agilent 1100 fluorescence detector and autosampler and ChemStation integration system. Wavelength settings were based on elution times with B[*a*]P-tetrols eluted between 10 and 20 min, two diols eluted between 20 and 27 min and B[*a*]P after 27 min. B[*a*]P metabolites were separated by a linear gradient of methanol and water, 30% methanol to 100% methanol in 40 min, followed by 10 min at 100% methanol and then 19 min at 30% methanol before the next injection.

2.7. DNA isolation and ^{32}P-postlabelling analysis

DNA from cells was isolated by the phenol extraction method as previously described [20]. ^{32}P-postlabelling analysis was carried out essentially as recently described with minor modifications [17]. Briefly, DNA samples (4 μg) were digested with micrococcal nuclease (120 mU, Sigma Chemical Co., Poole, UK) and calf spleen phosphodiesterase (40 mU, Calbiochem, Nottingham, UK). Resolution of ^{32}P-labelled adducts was carried out by chromatography on polyethyleneimine-cellulose (PEI-cellulose) TLC sheets (10 cm × 20 cm, Macherey-Nagel, Düren, Germany): D1, 1.0 M sodium phosphate, pH 6.0; D3, 3.5 M Li-formate, 8.5 M urea, pH 3.5; D4, 0.8 M LiCl, 0.5 M Tris, 8.5 M urea, pH 8.0. TLC sheets were scanned using a Packard Instant Imager (Dowers Grove, IL, USA) and DNA adduct levels (RAL, relative adduct labelling) were calculated from the adduct cpm, the specific activity of [γ-^{32}P]ATP and the amount of DNA (pmol of DNA-P) used. Results were expressed as DNA adducts/10^8 nucleotides. Benzo[*a*]pyrene-diol-epoxide (BPDE)-modified DNA

was included in the analysis as DNA adduct standard material [21].

2.8. Cell lysis and Western blotting

After treatment cells were washed twice in ice-cold PBS lysed in 20 mM Tris buffer, pH 7.5, 150 mM NaCl, 1 mM EDTA, 1 mM EGTA, 1% Triton X-100, 2.5 mM sodium pyrophosphate, 1 mM β-glycerol phosphate, 1 mM Na_3VO_4, 1 mM NaF, 10 mg/mL leupeptin, 1 mM PMSF, 10 mg/mL aprotinin and 10 mg/mL pepstatin A, sonicated and centrifuged. Protein concentration was measured using a Bio-Rad DC protein assay kit. Western blots were preformed as previously described [13]. Results from one representative experiment out of three are shown.

2.9. Measurement of pH_i

The pH_i of cells cultured on glass coverslips was monitored using the pH-sensitive fluorescent probe, carboxy-SNARF-1 (carboxy-seminaphtorhodafluor; Molecular Probes) [22], in HEPES-buffered solution which contained (in mM): NaCl 134.8, KCl 4.7, $MgCl_2$ 1.0, KH_2PO_4 1.2, $CaCl_2$ 1.0, glucose 10.0, HEPES (*N*-2-hydroxyethylpiperazine-*N*′-2-ethanesulphonic acid) 10, pH adjusted to 7.4 at 37 °C with NaOH. Cells were loaded with SNARF by incubating them in a 5 μM solution of the acetoxy-methyl ester for 20 min at 37 °C, just prior to performing the pH_i recording. SNARF-loaded cells were placed in a continuously perfused recording chamber (at a temperature of 36 ± 1 °C) mounted on the stage of an epifluorescent microscope (Nikon Diaphot). Cells were then excited with light at 514 nm and fluorescence from the trapped probe was measured at 590 and 640 nm. The necessary set-up to produce and detect the fluorescence has been previously described [23]. The emission ratio 640/590 (corrected for background fluorescence) detected from intracellular SNARF was calculated and converted to a linear pH scale using *in situ* calibration obtained by nigericin technique previously described [24].

2.10. Reactive oxygen species (ROS) detection

ROS production was assessed fluorometrically using oxidation-sensitive fluorescent probes, dihydroethidium (DHE, 5 μM, Molecular Probes) to detect $O_2^{\bullet -}$ and dichlorodihydro-fluorescein diacetate (H_2-DCFDA, 1 μM; Molecular Probes) to detect H_2O_2. For superoxide anion detection, cells were collected after a 20 or 48 h treatment, stained for 20 min at 37 °C with DHE (5 μM) in PBS and analyzed using a FACSCalibur flow cytometer (Becton Dickinson). For hydrogen peroxide detection, cells were stained with H_2-DCFDA during the 20 h treatment with B[*a*]P, collected after treatment and analyzed using the FACSCalibur flow cytometer. Pro-oxidants were used as positive controls: H_2O_2 (10 mM) for H_2-DCFDA and menadione (100 μM) for DHE. Each measurement was conducted on 10,000 cells and analyzed with Cell Quest Software (Becton Dickinson). Four independent experiments were carried out.

2.11. Mitochondrial membrane potential

Modifications in mitochondrial membrane potential were detected using the fluorescent probe $DiOC_6$ (3,3′-dihexyloxacarbocyanine iodide, Molecular Probes). After 20 or 48 h treatment, cells were collected and stained with 50 nM $DiOC_6$ (Molecular Probes) in PBS for 20 min at 37 °C. FCCP (mesoxalonitrile 4-trifluoromethoxyphenylhydrazone; 50 μM) was used as positive control. Analysis was performed using the FACSCalibur flow cytometer.

2.12. Immunocytochemistry

Cells were seeded at low density into 35 mm dishes on glass coverslips and treated. After washing in PBS, adherent cells were fixed on coverslips with 4% paraformaldehyde in PBS for 30 min at 4 °C and washed three times with PBS. Then, cells were incubated for 1 h with a blocking-permeabilizing solution (0.2% saponin–0.2% BSA in PBS). After washing, cells were incubated with either rabbit anti-Bax or rabbit anti-cytochrome *c* primary antibody and mouse monoclonal anti-COX IV (clone 1D6) in a blocking-permeabilizing solution for 2 h at room temperature, washed in PBS and then stained with TRITC-conjugated anti-rabbit IgG and FITC-conjugated anti-mouse IgG, respectively, for 1 h at room temperature. Thereafter, cells were co-stained by a 15 min incubation in a blocking solution containing 1 μg/mL DAPI, a fluorescent dye specific for DNA. After washing, coverslips were mounted with PBS-glycerol-Dabco. Fluorescent-labelled cells were captured with a DMRXA Leica microscope and a COHU high performance CCD camera, using Metavue software. Data are representative of, at least, three independent experiments.

2.13. Statistical method

Statistical comparisons were carried out using a Student's *t*-test for unpaired two-tailed, comparisons.

A p-value of less than 0.05 was considered significant.

3. Results

In the Hepa1c1c7 model, cells are normally cultured at high, near confluent cell density (90×10^3 cells/cm^2), exposed to 10–20 μM B[a]P and apoptosis is measured over a period of 24 h; whereas in the F258 model, cells are normally cultured at low density (2.5×10^3 cells/cm^2), exposed to 50 nM B[a]P and apoptosis develops over a period of 48–72 h. In the present study we compare and elucidate mechanisms involved in B[a]P-induced toxicity in Hepa1c1c7 and F258 cells cultured both at low and high cell density for direct comparison.

3.1. Sensitivity to B[a]P

The two cell lines were seeded at low and high cell density and exposed to different concentrations of B[a]P. No toxic effects were observed in F258 cells after 24 h exposure to B[a]P 0.05–20 μM, when plated at low or high density (data not shown). However, when F258 cells seeded at low cell density were exposed to 50 nM B[a]P for 48 h, 8–11% of the cells become apoptotic. A further increase was seen with 5 μM B[a]P, and following 20 μM rather a decrease in cell death (Fig. 1). At high cell density only a small increase in cell death in F258 cells was observed at the two highest concentrations tested after 48 h exposure.

In Hepa1c1c7 cells cultured at low cell density, most of the cells were dead following 24 h exposure to 5 and 20 μM B[a]P (data not shown), and at 50 nM B[a]P a small and somewhat variable effect could be seen after 48 h of exposure (3–5%, Fig. 1). At high cell density, only 20 μM B[a]P induced marked cell death (20–30% mixture of apoptotic and necrotic cells) after 24 h as previously reported, whereas after 48 h a marked increased was also observed with 5 μM B[a]P.

3.2. Metabolism of B[a]P

B[a]P is metabolized into a number of different metabolites, including hydoxylated metabolites and different diols which can be further conjugated or metabolized into reactive diol-epoxides (BPDE-I and BPDE-II) that can initiate toxic effects. In order to elucidate any possible role of B[a]P metabolism, metabolites

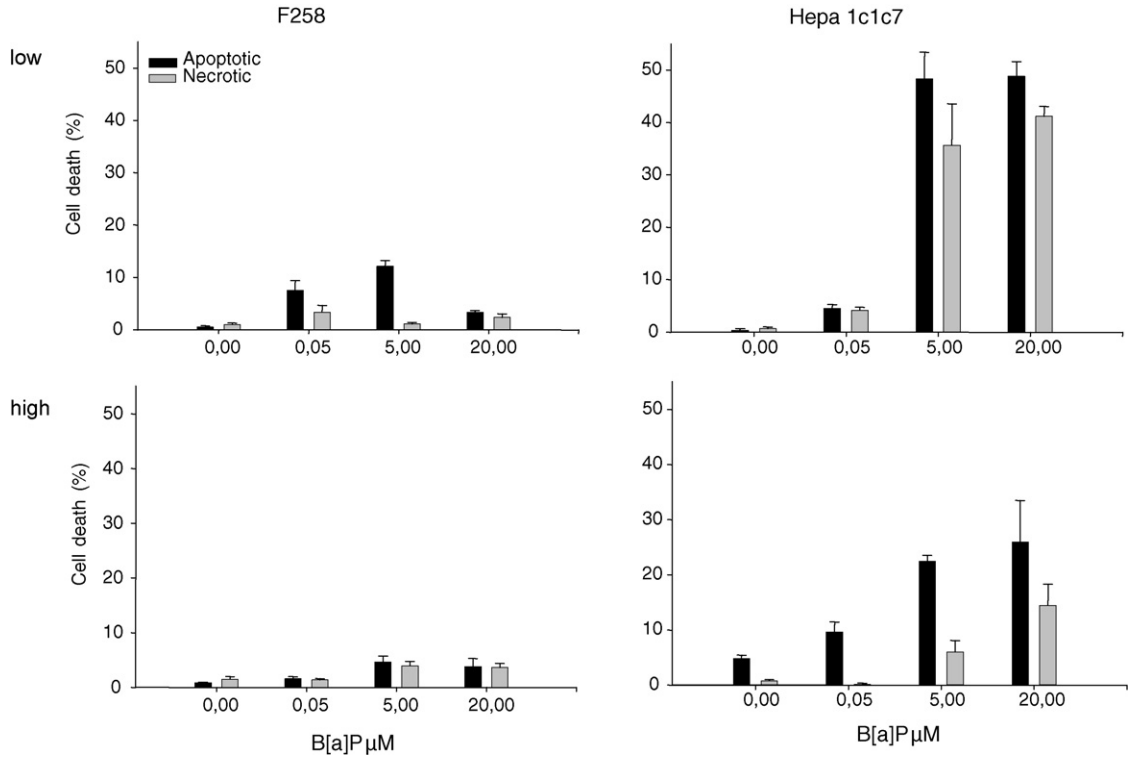

Fig. 1. Effects of B[a]P on cell death. F258 cells and Hepa1c1c7 cells were seeded at low (2.5×10^3 cells/cm^2) or high (90×10^3 cells/cm^2) cell densities and treated with various concentrations of B[a]P for 48 h. The results are from fluorescence microscopic analysis and presented as % apoptotic cells and necrotic cells. The data are means ± S.D. of three separate incubations from a representative experiment.

Table 1
Generation of B[*a*]P metabolites in F258 and Hepa1c1c7 cells

B[*a*]P metabolites	F258		Hepa1c1c7	
	3 μM	10 μM	3 μM	10 μM
B[*a*]P-3-OH	1.09 ± 0.05	1.96 ± 0.27	115.05 ± 20.56[a]	798.34 ± 32.46[a]
B[*a*]P-9-OH	4.46 ± 0.14	3.37 ± 0.18	3.63 ± 0.60	62.91 ± 1.87[a]
B[*a*]P-7,8-DHD	1.11 ± 0.06	1.41 ± 0.20	6.61 ± 0.04[a]	49.00 ± 13.38[a]
B[*a*]P-4,5-DHD	0.00 ± 0.00	1.69 ± 0.10	18.21 ± 0.84[a]	52.07 ± 0.22[a]
B[*a*]P-tetrol-I-1	0.00 ± 0.00	0.00 ± 0.00	13.40 ± 1.28[a]	53.21 ± 1.56[a]
B[*a*]P-tetrol-II-1	0.00 ± 0.00	0.00 ± 0.00	1.34 ± 0.26[a]	6.58 ± 1.25[a]
B[*a*]P-tetrol-I-2	0.00 ± 0.00	0.00 ± 0.00	0.76 ± 0.13[a]	6.31 ± 0.50[a]
B[*a*]P-tetrol-II-2	0.00 ± 0.00	0.00 ± 0.00	0.60 ± 0.05[a]	4.06 ± 0.63[a]

F258 and Hepa1c1c7 cells (90×10^3 cells/cm^2) were incubated with B[*a*]P (3 or 10 μM) for 7 h. The supernatant were then treated with deconjugation-enzymes and the B[*a*]P metabolites were purified on Sep-pak C_{18} cartridges before quantitative determination by fluorescence HPLC. The data are mean of final B[*a*]P metabolite concentration in cell medium (nM) ±S.E. of three parallel incubations.

[a] Indicate that values in the F258 cells for the respective B[*a*]P metabolite are statistically different from the Hepa1c1c7 cells.

formed by the two cell lines were analyzed. Based on preliminary studies, high cell density, high B[*a*]P concentration and an exposure time of 7 h was chosen. Under these conditions the parent compound remained in both cultures, and enough B[*a*]P metabolites were formed to allow HPLC analysis. Before analysis of the medium, conjugated metabolites were hydrolyzed. As can be seen from the data presented in Table 1 and Fig. 2, the total rate of B[*a*]P metabolism in Hepa1c1c7 cells was much higher than that observed in F258 cells. Depending on the concentration, the formation of the most prominent metabolite, B[*a*]P-3-OH, was in the range 100–1000 times higher in Hepa1c1c7 cells than in F258 cells, while the levels of B[*a*]P-9-OH were rather similar. A much higher rate of formation of the B[*a*]P-7,8-DHD and B[*a*]P-4,5-DHD in Hepa1c1c7 cells was also observed. Furthermore, the hydrolysis products of the reactive BPDE-I and BPDE-II metabolites, the tetrols, were only observed in Hepa1c1c7 cells.

In order to explore possible mechanisms involved in the apparent long delay of B[*a*]P-induced cell death in the F258 cells model (no cell death in F258 cells was observed before 48 h after onset of B[*a*]P exposure), we estimated the period of initial damage formation by measuring the removal of 50 nM B[*a*]P from the medium. As can be seen in Fig. 2B the half-life of B[*a*]P in F258 cells was in the order of 24 h. No marked (some caused by an increased number of cells) time-dependent increase in the rate of metabolism could be observed.

To further compare the formation of reactive B[*a*]P metabolites in the two cell lines DNA adducts as measured by the ^{32}P-postlabelling technique, were analyzed in proliferating cells. Both F258 and Hepa1c1c7 cells were able to metabolize B[*a*]P to reactive metabolites which covalently bind to DNA (Fig. 3). The main adduct formed in both cell lines was identified as dG-N^2-BPDE, which is considered to result from the reactive BPDE-I. In F258 cells, the level of DNA adducts following exposure to various concentrations of B[*a*]P (1, 5 and 10 μM) were similar. Somewhat less adducts were seen at 1 μM B[*a*]P in Hepa1c1c7 cells, partly due to a complete metabolism of B[*a*]P following the relative long incubation time used (15 h), whereas exposure to 5 and 10 μM increased the level of DNA adducts by a factor of up to 13.

Since there seemed to be major differences between the two cell lines with regard to metabolic activation of B[*a*]P, we examined the levels of cyp1a1 and cyp1b1 following exposure to B[*a*]P. cyp1a1 was not observed in the F258 cells, whereas cyp1b1 was detected but not markedly induced by B[*a*]P as judged by Western analysis (Fig. 4). In Hepa1c1c7 cells a large induction of cyp1a1 could be observed (already at 8 h; data not shown) following exposure to B[*a*]P (Fig. 4). The level of cyp1b1 was, however, not induced under the present experimental conditions and the constitutive level in Hepa1c1c7 cells was apparently lower than in F258cells (Fig. 4).

3.3. Effects on intracellular pH (pH_i)

We have previously shown that low concentrations of B[*a*]P increase the intracellular pH in F258 cells, and that this increase modulate the apoptotic response [15]. The data in Fig. 5A shows the effect of a high concentration (20 μM) of B[*a*]P on the two cell lines at various times after start of exposure. In both F258 as well as Hepa1c1c7 cells, B[*a*]P caused a rapid increase in pH_i that peaked after 6 h and normalized after 22 h. When the cells were cultured at high cell density, no significant effects on pH_i were observed whatever cell line used (Fig. 5B). To

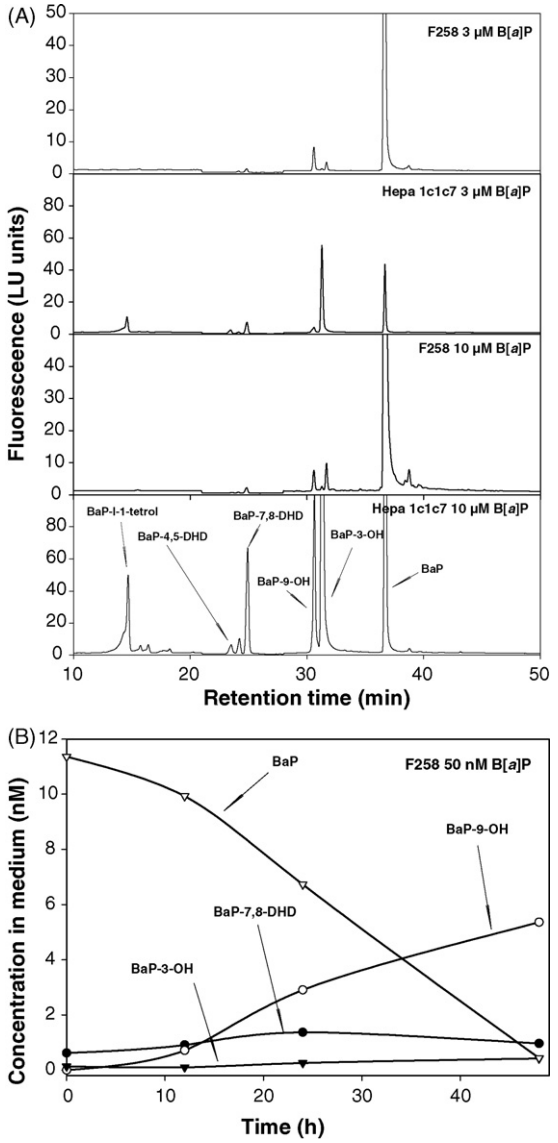

Fig. 2. (A) HPLC analysis of B[*a*]P metabolites from F258 and Hepa1c1c7 cells. F258 and Hepa1c1c7 cells (90×10^3 cells/cm^2) were exposed to various concentrations of B[*a*]P for 7 h. The supernatant were then treated with deconjugation-enzymes and the B[*a*]P metabolites were purified on Sep-pak C_{18} cartridges before quantitative determination by fluorescence HPLC. (B) Time-dependent metabolism of B[*a*]P (50 nM) in F258 cells. F258 cells were seeded at low cell density (2.5×10^3 cells/cm^2) and exposed to low concentration of 50 nM B[*a*]P for various time periods. Supernatants were concomitantly analyzed as described above.

examine the role of NHE1-dependent alkalinization in B[*a*]P-induced apoptosis, we co-exposed cells (seeded at low density) to low concentrations of B[*a*]P (100 and 300 nM; which give a clear induction of cell death in both cell lines) and cariporide (30 μM; a specific inhibitor of NHE1), and estimated the number of apoptotic cells. Fig. 5C and D support data in Fig. 1, that F258 cells are somewhat more sensitive than Hepa1c1c7 cells at low concentrations (50 and 100 nM) of B[*a*]P. Furthermore, they show that while, as expected, the number of cell death was significantly inhibited by cariporide in F258 cells, no marked effects of cariporide were seen in Hepa1c1c7 cells under these conditions.

3.4. Formation of ROS and mitochondrial damages

ROS may be formed during B[*a*]P metabolism as well as during the cell death process as a result of induced mitochondrial damage, and has been found to be of importance for the B[*a*]P induced increase in pH_i observed in the F258 cell model [15]. To measure the formation of H_2O_2, we used the fluorescent probe H_2DCF-DA following 20 h exposure to various concentrations of B[*a*]P at low cell density (a density which allows toxicity to develop in both cell models). Specific differences in the production were detected between the two cell lines: an increase in H_2O_2 without any apparent toxicity was observed from 50 nM B[*a*]P in F258 cells, while no such increase was observed at this low concentration of B[*a*]P in Hepa1c1c7 cells. At 5 and 20 μM B[*a*]P a large increase of H_2O_2 formation in Hepa1c1c7 cells was seen (Fig. 6A), however, this increase was most probably due to secondary mitochondrial effects as often found during cell death. Furthermore, unlike F258 cells, no effects of antioxidants were found in Hepa1c1c7 cells (data not shown).

Superoxide anion production was quantified at two treatment times and with low cell density. As previously reported, a 20 h treatment with B[*a*]P induced a small increase in $O_2^{\bullet -}$ production in F258 cells, evidenced by the rightward shift of the DHE fluorescent peak of treated cells [23]. In these cells, the increase was in the same range whatever the concentration of B[*a*]P. Regarding Hepa1c1c7 cells, no such increase was detected following 20 h even at the highest concentrations (Fig. 6B). After 48 h treatment, the B[*a*]P induced increased $O_2^{\bullet -}$ production in F258 cells was more marked. In Hepa1c1c7 cells low B[*a*]P concentration (50 nM) still had no effect, whereas at the highest concentrations, the $O_2^{\bullet -}$ concentration was decreased in the cell population consisting mostly of dead cells.

Mitochondrial membrane polarization was analyzed using a fluorescent probe, sensitive to mitochondrial membrane potential (Fig. 7). After exposure to B[*a*]P for 20 h, a small hyperpolarization was detected in F258 cells, as evidenced by the rightward shift of $DiOC_6$ fluorescent peak of treated cells as also reported elsewhere [23]. The hyperpolarization was in the same range at all

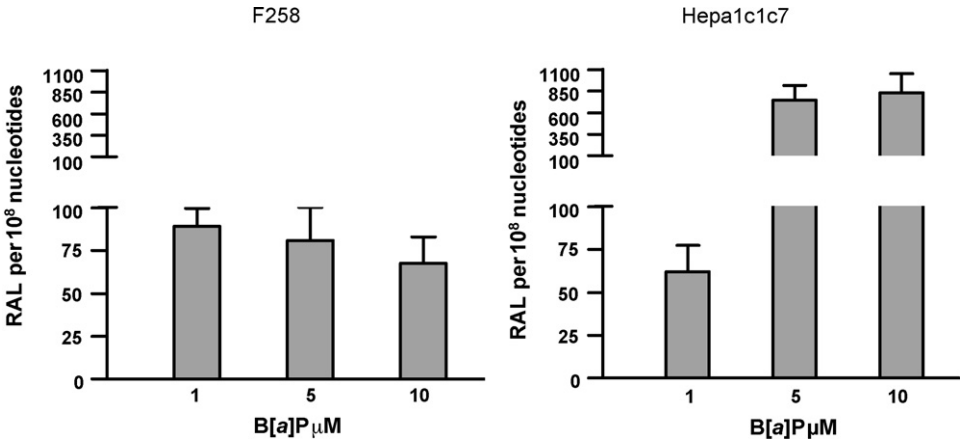

Fig. 3. ^{32}P-postlabelling analysis of DNA from cells exposed to B[*a*]P. Levels of DNA adducts (dG-N^2-BPDE) were measured in F258 and Hepa1c1c7 cells (20×10^3 cells/cm^2) after exposure for 15 h to different concentrations of B[*a*]P using the nuclease P1 enrichment version of the ^{32}P-postlabelling assay. Values represent mean ± S.D. of three separate incubations each determined by two independent postlabelling analyses.

B[*a*]P concentrations tested. In Hepa1c1c7 cells, 50 nM B[*a*]P had no effect on mitochondrial membrane polarity, while a slight hyperpolarization was seen in cells treated with high concentrations of B[*a*]P (5 or 20 μM). Following 48 h, a stronger hyperpolarization was detected in F258 cells. Regarding Hepa1c1c7 cells, whereas no effect was detected at 50 nM B[*a*]P, a strong depolarization (leftward shift of $DiOC_6$ fluorescent peak) was then detected, corresponding to dead cells.

The Bcl-2 family proteins are important regulators of mitochondrial membrane potential and apoptosis. Previous studies have indicated that they may have different roles in the two models (F258 cells cultured at low cell density and exposed to low concentrations of B[*a*]P *versus* Hepa1c1c7 cells at high cell density and exposed to high concentrations of B[*a*]P). The data in Fig. 8A show that the level of Bax in F258 cells remained unchanged after exposure to 50 nM of B[*a*]P; however, at 5 and 20 μM, level of Bax was somewhat increased. Nevertheless, no change of Bax localization was observed upon B[*a*]P exposure (Fig. 8B). In Hepa1c1c7 cells seeded at high cell density, B[*a*]P (20 μM) caused no change in the level of Bax (Fig. 8A), but a marked translocation to the mitochondria could be observed both at low (Fig. 8B) as well as high cell density [13]. In F258 cells, only a minor increase in pro-apoptotic Bad and a corresponding decrease in p-Bad was observed at 20 h. After 48 h, a minor decrease in the levels of Bcl-x_L was detected at the two highest concentrations, while rather an increase in the phosphorylation of Bad could be seen (Fig. 8A). As also published in previous studies [13], the level of Bcl-x_L decreased and phosphorylation of Bad increased in Hepa1c1c7 cells exposed to 20 μM B[*a*]P (Fig. 8A). A release of cytochrome *c* from the mitochondria in the Hepa1c1c7 model was visualized by fluorescence microscopic analysis, whereas in the F258 model, B[*a*]P caused no such changes (Fig. 8B).

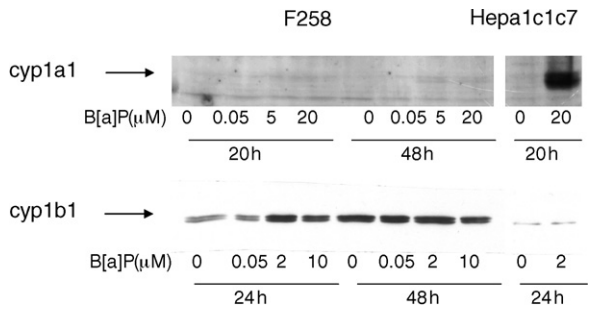

Fig. 4. Effects of B[*a*]P on cyp1a1 and cyp1b1 expression. F258 cells seeded at low cell density (2.5×10^3 cells/cm^2) were incubated with various B[*a*]P concentrations for 20 and 48 h and analyzed for cyp1a1 and cyp1b1 expression by Western blotting. Hepa1c1c7 cells exposed to B[*a*]P (2 and 20 μM) for 25 h were used as control. Results from one representative experiment of at least three are shown.

3.5. *Effects on cell survival signals*

We have previously found that various cell survival signals including p-ERK1/2 and p-Akt are induced in Hepa1c1c7 cells following exposure to B[*a*]P [13]. Here we exposed F258 cells cultured at low cell density to both low and high concentrations of B[*a*]P (Fig. 9). Whereas p-Akt in the Hepa1c1c7 cell model were somewhat increased following exposure to B[*a*]P, rather a decrease in both p-ERK1/2 and p-Akt was observed in F258 cells following 20 and 48 h. In both unexposed and exposed F258 cells, a small increase in the phosphorylation of Akt was observed at 48 h when compared to 20 h. The effect of B[*a*]P on pERK1/2 in the Hepa1c1c7 cells

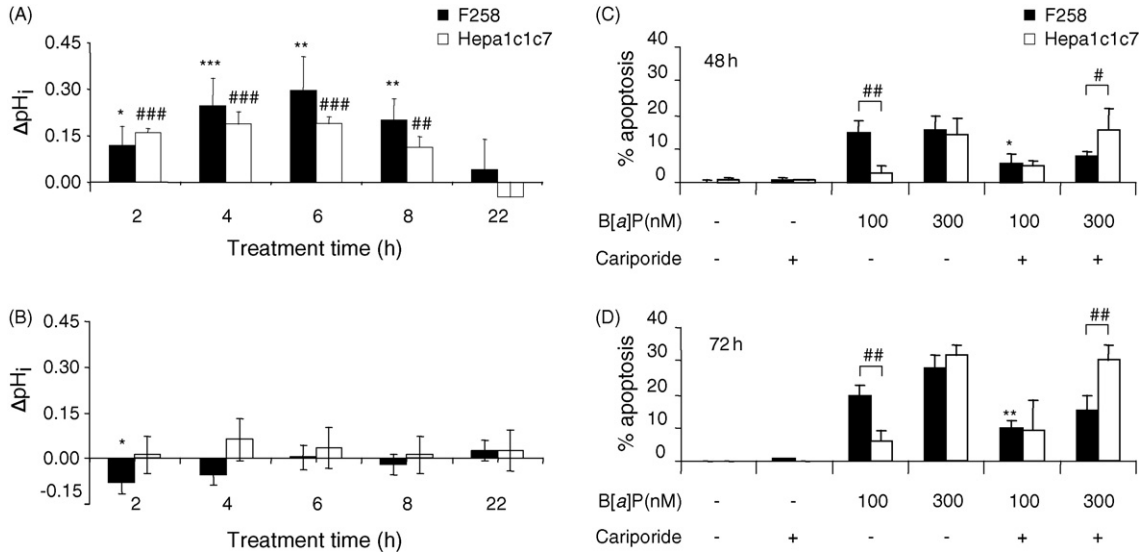

Fig. 5. Effects of B[*a*]P on intracellular pH. (A and B) Effects of B[*a*]P on intracellular pH. F258 and Hepa1c1c7 cells were seeded at low (2.5×10^3 cells/cm^2; A) or high (90×10^3 cells/cm^2; B) cell densities and treated with 20 μM of B[*a*]P for 2–22 h. pH_i measurements were performed using the pH-sensitive fluorescent probe, carboxy-SNARF-1. The graph represents the mean ± S.E.M. of ΔpH_i ($pH_{i(conrol)} - pH_{i(B[a]P)}$) of four (F258) or six (Hepa1c1c7) independent experiments. $^{\#/*}p < 0.05$, $^{\#\#/**}p < 0.01$, $^{\#\#\#/***}p < 0.001$: control *vs.* B[*a*]P. (C and D) Involvement of B[*a*]P-induced alkalinization in apoptosis. Hepa1c1c7 and F258 cells, seeded at low cell density (2.5×10^3 cells/cm^2), were treated or not with B[*a*]P (100 or 300 nM) in the presence (+) or absence (−) of 30 μM cariporide for 48 h (C) or 72 h (D). After collection and staining with Hoechst 33342, the percentage of apoptotic cells was obtained by fluorescence microscopy analysis of chromatin condensation and fragmentation. Results are given as mean ± S.E.M. of three (F258) or five (Hepa1c1c7) independent experiments. $^{*}p < 0.05$: B[*a*]P *vs.* cariporide + B[*a*]P. $^{\#}p < 0.05$, $^{\#\#}p < 0.01$: Hepa1c1c7 cells *vs.* F258 cells.

was somewhat varying. At somewhat lower concentrations of B[*a*]P (1 and 10 μM) an increase was most often observed at 20 h (data not shown), whereas at 20 μM more often a slight decrease was seen.

4. Discussion

Cell death such as apoptosis protects the tissue from effects of carcinogens by removing cells with extensive DNA damage and by balancing cell proliferation. DNA damage often initiates a number of various cell signaling pathways related to DNA repair activity, cell cycle arrest and cell survival or cell death (apoptosis). The relative proportion of the different cell signaling pathways triggered by DNA damage upon exposure will to a large degree determine if the compound is mutagenic or mostly give cytotoxic effects.

Separate studies have suggested that B[*a*]P induces apoptosis in the F258 model and in the Hepa1c1c7 model through different mechanisms. Here, we compare the two cell lines directly and elucidate possible mechanisms. Large differences with regard to sensitivity to B[*a*]P-induced apoptosis were seen at the two cell densities used. When cultured at low cell density and exposed to low B[*a*]P concentrations (50 and 100 nM) F258 cells seem to be somewhat more sensitive than Hepa1c1c7 cells (Figs. 1 and 5), while at higher concentrations much more cell death was induced in Hepa1c1c7. These differences are partly explained by the results obtained from the studies on B[*a*]P metabolism. In general, a much higher rate of metabolism was found in Hepa1c1c7 cells, which is in accordance with the higher level of induced cyp enzymes found. The high level of 3-OH-B[*a*]P when compared to 9-OH-B[*a*]P found in Hepa1c1c7 cells is well in accordance with the finding that cyp1a1 was the major cyp enzyme in these cells, since the same metabolic profile has been reported following B[*a*]P metabolism using cloned cyp1a1 [25]. Similarly, the relative low 3-OH-B[*a*]P/9-OH-B[*a*]P ratio found in F258 cells correspond well with the metabolite pattern of the cyp1b1 enzyme [26], which we found to be the dominating cyp isoform in these cells.

The rate of formation of reactive metabolites at higher B[*a*]P concentrations, as judged by the measurement of tetrols and DNA adducts, was higher in Hepa1c1c7 than in F258 cells giving an explanation to the finding that Hepa1c1c7 cells were the more sensitive cell line at these concentrations. Thus, acute toxicity of B[*a*]P (observed after 24 h) seems to be triggered if a large amount of DNA reactive metabolites formed over a short period

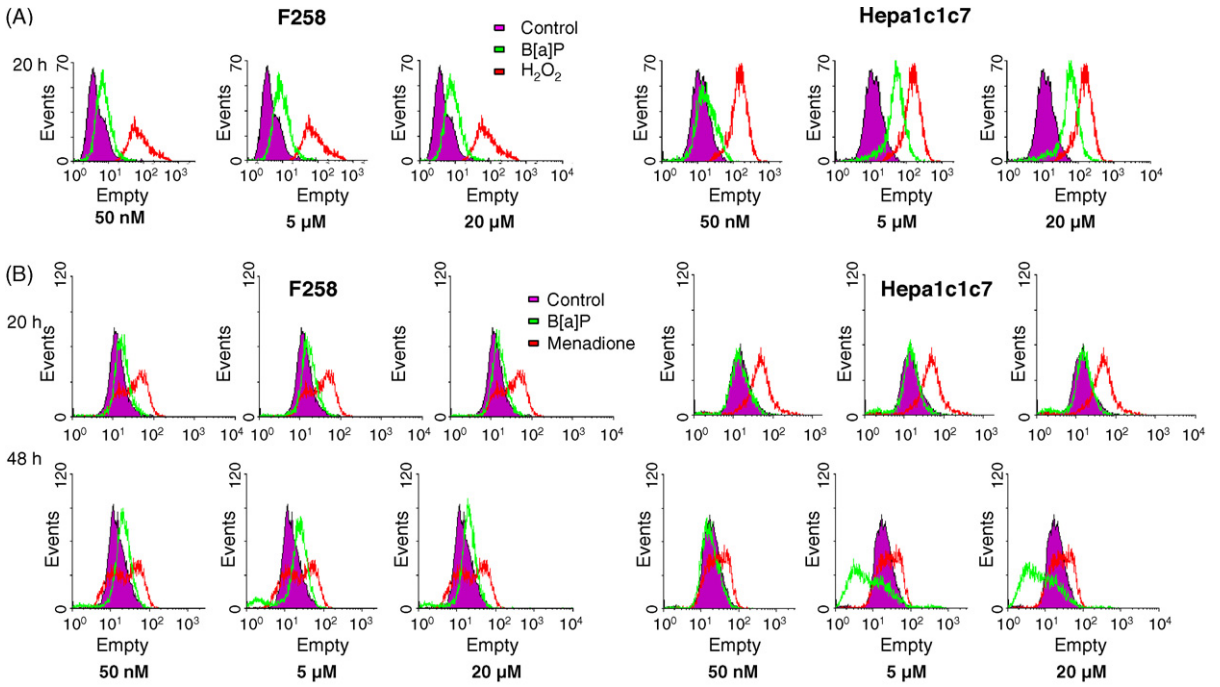

Fig. 6. (A) B[*a*]P induces hydrogen peroxide production. Cells, seeded at low cell density (2.5×10^3 cells/cm^2), were treated (B[*a*]P) with B[*a*]P (50 nM, 5 μM or 20 μM) or not (control) for 20 h. H_2O_2 production was analyzed using H_2-DCFDA and flow cytometry. A 20 min treatment with H_2O_2 was used as positive control for ROS production. Peaks are representative of three independent experiments. (B) B[*a*]P induces superoxide anion production. Cells, seeded at low cell density (2.5×10^3 cells/cm^2), were treated (B[*a*]P) with B[*a*]P (50 nM, 5 μM or 20 μM) or not (control) for 20 or 48 h. $O_2^{\bullet -}$ production was analyzed using DHE and flow cytometry. A 20 min treatment with menadione was used as positive control for ROS production. Peaks are representative of three independent experiments.

of time. The B[*a*]P-DNA adducts found in the present study most probably initiate the ATM/ATR and p53-dependent apoptosis described previously [14]. In the F258 model, B[*a*]P-induced apoptosis was first observed 48–60 h after onset of exposure. Taken into consideration the higher metabolic rate and capacity found in Hepa1c1c7 cells compared to F258 cells, the finding that the F258 cells seemed to be slightly more sensitive than Hepa1c1c7 cells to low B[*a*]P concentrations at low cell density may at first appear surprising. However, in a process that develops over a long period (48 h), most of the B[*a*]P is metabolized also in F258 culture. In this case

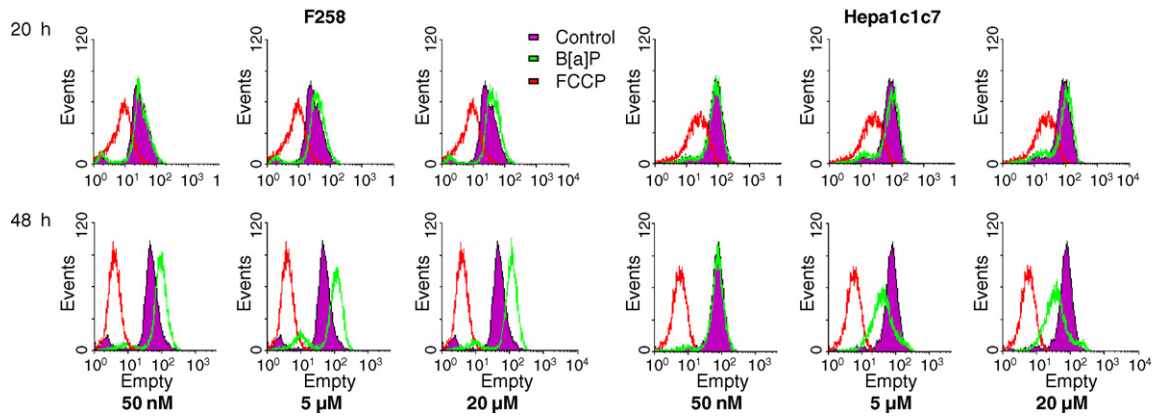

Fig. 7. Effects of B[*a*]P on mitochondrial membrane potential. Cells, seeded at low cell density (2.5×10^3 cells/cm^2), were treated with B[*a*]P (50 nM, 5 μM or 20 μM) or not (control) for 20 or 48 h. The mitochondrial membrane potential was analyzed using $DiOC_6$ and flow cytometry. A 20 min treatment with the decoupling agent FCCP was used as positive control for ROS production. Peaks are representative of three independent experiments.

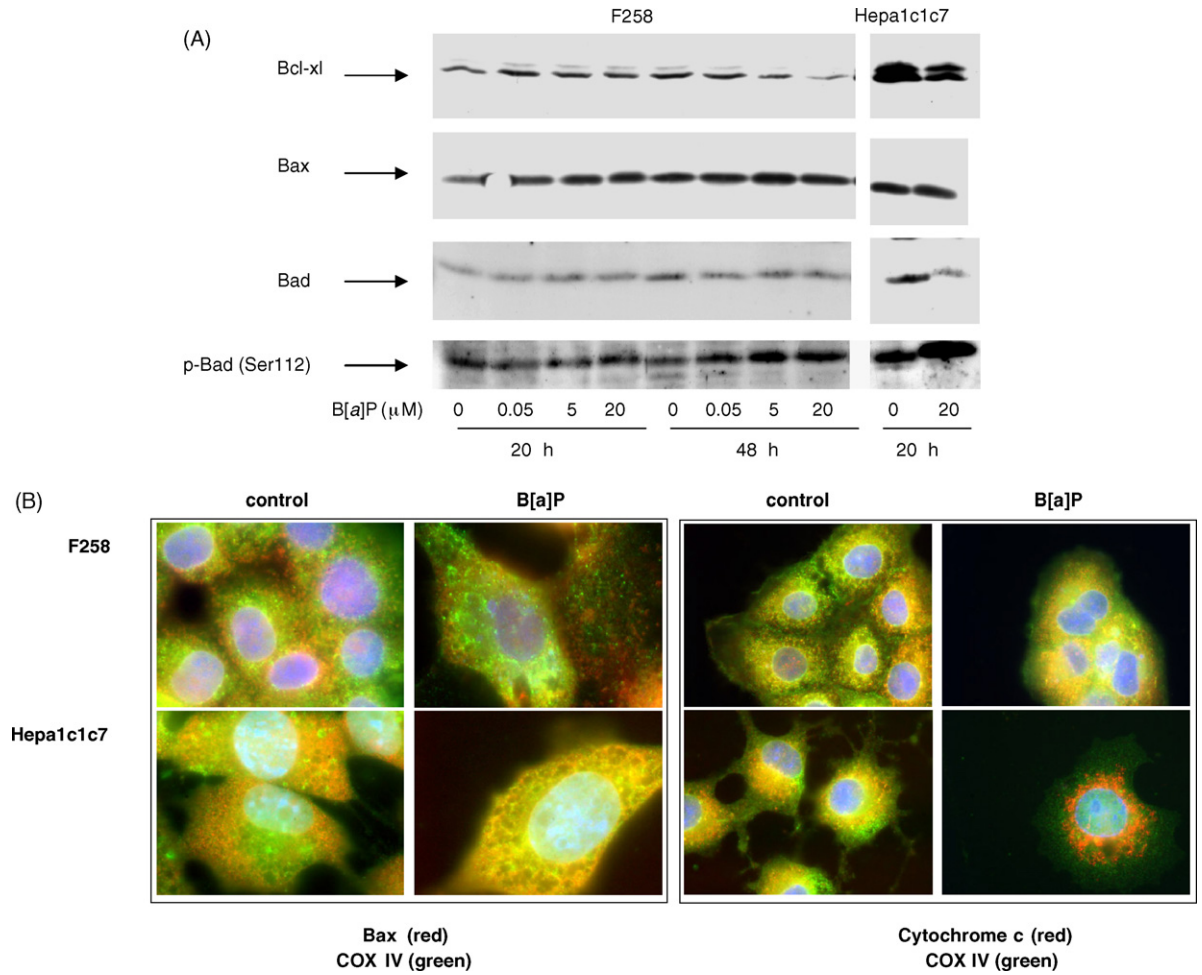

Fig. 8. (A) Expression of different Bcl-2 proteins following exposure to B[*a*]P. F258 cells seeded at low cell density, were incubated with different concentrations of B[*a*]P for 20 and 48 h and analyzed for expression of Bcl-x_L, Bax, Bad phosphorylated at Ser112 and total Bad by Western blotting. Hepa1c1c7 cells seeded at high cell density and treated with B[*a*]P (20 μM, 20 h) were used as a positive control. Results from one representative experiment out of three are shown. (B) Localization of cytochrome *c* and Bax following B[*a*]P exposure. F258 and Hepa1c1c7 cells, seeded at low cell density, were treated or not with 3 μM B[*a*]P during 48 h. After fixation and permeabilization, cells were co-immunostained with a rabbit primary antibody (secondary stained with TRITC-conjugated anti-rabbit IgG) and a mouse primary antibody (secondary stained with FITC-conjugated anti-mouse IgG); detecting mouse anti-COX IV were used as mitochondrial marker. On the left panel, cells are labelled with rabbit anti-Bax (red) and mouse anti-COX IV (green). On the right panel, cells are labelled with rabbit anti-cytochrome *c* (red) and mouse anti-COX IV (green). Co-localization of the two antibodies results in yellow fluorescence. Cells were co-stained with DAPI (blue) to detect nuclei. The pictures are representatives of three independent experiments.

the determining factor will not be the rate of formation of reactive metabolites, but more the total amount of DNA reactive metabolites formed from the B[*a*]P added (accumulated DNA damage). In accordance with this hypothesis, it is noteworthy that slightly higher DNA adduct levels were found in F258 cells at rather low concentrations of B[*a*]P (1 μM) following a longer (15 h) incubation time. Furthermore, although Hepa1c1c7 cells have the highest rate of formation of reactive metabolites a much larger fraction of the total metabolites formed represents the detoxified metabolite B[*a*]P-3-OH. Also possible differences in the two cell lines with regard to GSH/GST activities could have a role.

In accordance with the suggestions from the metabolism studies, Western blot analysis revealed that cyp1b1 appears to dominate in F258 cells, whereas in Hepa1c1c7 cells cyp1a1 seems to dominate at least in the induced state. Although both enzymes can activate B[*a*]P, it is often considered that cyp1a1 is important in the first metabolic activation step of B[*a*]P, whereas cyp1b1 is more involved in the further activation of B[*a*]P-7,8-DHD [26]. In CH3T101/2 cells

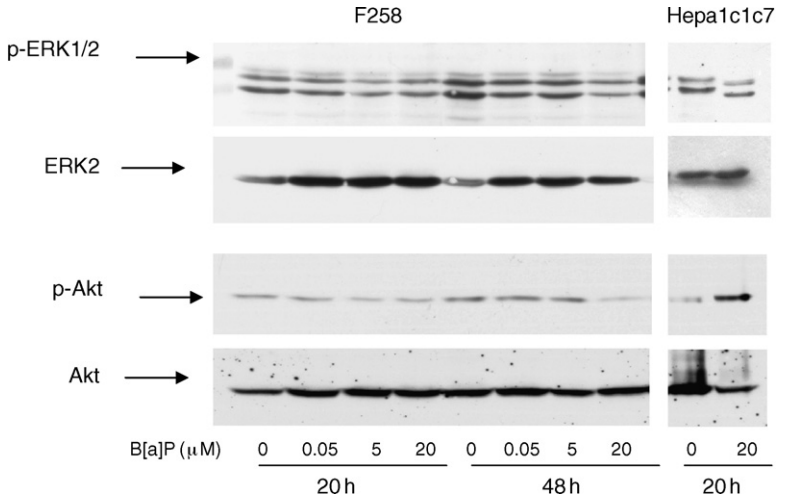

Fig. 9. Effects of B[*a*]P on phosphorylation of ERK1/2 and Akt. F258 cells, cultured at low cell density, were incubated with different concentrations of B[*a*]P for 20 and 48 h and analyzed for expression of p-ERK1/2 and p-Akt by Western blotting. Hepa1c1c7 cells, cultured at high cell density treated with B[*a*]P (20 μM, 20 h) were used as a positive control. Results from one representative experiment out of three are shown.

cyp1b1 metabolizes B[*a*]P into B[*a*]P-DHD and further into the reactive B[*a*]P-DHDE [27]. Interestingly, these cells also further activate B[*a*]P-DHD by dihydrodiol-dehydrogenases to catechols, which form ROS following recycling, thus contributing to the toxic response. When taking into consideration that ROS seem to be an important part of the B[*a*]P-initiating apoptotic signal in F258 cells [15], one might anticipate that dihydrodiol-dehydrogenase could have a similar function in F258 cells. In the present study, however, no major uncharacterized B[*a*]P metabolites (*e.g.* catechols, quinones and semiquinones) were detected in the incubation medium of F258 cells that could further substantiate this suggestion. However, the apparent lack of quinone-metabolites does not exclude the possibility that they are formed, as they often have lower fluorescence and are thus hard to detect [28].

In the F258 model, ROS and in particular H_2O_2 have been suggested to be important initiating signals resulting in an NHE1-dependent early alkalinization [15]. Experiments performed using microspectrofluorimetry and the pH-sensitive fluoroprobe carboxy-SNARF-1 indicate that high concentrations of B[*a*]P induces pH_i changes in Hepa1c1c7 cells in a range similar to those observed in F258 cells if incubated at low cell density. A common step for the NHE1 activation could be phosphorylation of JNK, as activation of JNK is observed in both cell lines [14] (Huc et al., unpublished data). However, despite similar pH_i changes, the addition of the NHE1-inhibitor cariporide, did not reduce the PAH-induced apoptosis in Hepa1c1c7 suggesting that the induced alkalinization was not an essential step in the induced apoptosis in these cells.

ROS production has previously been shown to be linked to B[*a*]P metabolism and to be an important initial apoptotic event in F258 cells [15,23]. Some ROS production was also detected in Hepa1c1c7 cells, but only following exposure to high B[*a*]P concentrations and at time points with high cell death. Taken into consideration that antioxidants had no effects (data not shown), and that ROS are often formed during the process of chemical-induced apoptosis and necrosis [29], this finding does not suggest that the initial toxic insults in Hepa1c1c7 cells are related to ROS.

There were also marked differences between the two cell lines with regard to mitochondrial changes. In F258 cells, B[*a*]P induced a stable increase in the $O_2^{\bullet -}$ production and hyperpolarization of mitochondria. In contrast, B[*a*]P decreased the level of $O_2^{\bullet -}$ and caused mitochondrial depolarization at high concentrations in Hepa1c1c7, whereas at low concentrations no marked effects were seen. The mitochondrial hyperpolarization seen in F258 cells is often found to be an early apoptotic change following exposure to various chemicals [30,31]; however, in some cases, such an hyperpolarization has also been suggested to constitute a survival signal [28]. This is presently under investigation.

In the Hepa1c1c7 model, B[*a*]P-induced apoptosis is initiated by DNA damage possibly sensed by ATM/ATR and Chk2 kinases, which phosphorylate and stabilize p53, thereby further triggering both the intrinsic as well as the extrinsic apoptotic pathways apparently in a rather

"classical" way. The phosphorylation of p53 at serine 15 has been shown to be important for *trans*-activation activity of p53 and has been suggested to represent an early response to a variety of genotoxic stress [32]. Furthermore, mutations in serine impaired the apoptotic activity of p53 [33] suggesting a pivotal role for serine 15 phosphorylation in the induction of apoptosis. Recent studies also suggest a central role for induced p53 phosphorylation in the F258 model, although implications of initiator caspases 8 or 9 have been questioned [16]. A role of p53 related to activation of Puma, Noxa, and caspase-2 have been reported in other experimental systems [11] and would deserve further investigation in F258 cells.

The Bcl-2 proteins are known to regulate the mitochondria or intrinsic apoptotic pathway, and changes in the relative amount or intracellular location of these proteins may elicit the release of cytochrome *c*, an event resulting in caspase-3 activation and apoptosis. In the present study, B[*a*]P did not change the levels of the Bcl-2 family members Bcl-2 (data not shown) or Bax, while a down-regulation of Bcl-x_L was seen in Hepa1c1c7 cells. It is noteworthy that no change was seen in F258 cells at low concentrations of B[*a*]P. In Hepa1c1c7 cells, B[*a*]P induced a translocation of Bax from the cytosol to the mitochondria as often seen with pro-apoptotic members following activation of p53, whereas no such translocation could be seen in the F258 cell model. Furthermore, we here show that cytochrome *c* was released from the mitochondria in Hepa1c1c7 cells during B[*a*]P-induced apoptosis pointing to a rather "classical way", while no such change could be observed in F258 cells, thus extending and corroborating previous results [13,16,14].

Previous studies with the Hepa1c1c7 cell line have suggested specific triggering of cell survival signals and inhibition of pro-apoptotic signals following exposure to B[*a*]P [12,13]. B[*a*]P as well as its DNA reactive metabolites have been found to result in a down-regulation and a correspondingly increased phosphorylation of Bad at Ser112 and/or Ser155. This phosphorylation reduces Bad capacity to form heterodimers and can thereby be considered as a cell survival signal [34,35]. Furthermore, an increased phosphorylation of ERK and Akt which both are considered to be important cell survival signals [35–37], are observed following exposure to B[*a*]P and may possibly also be involved in the triggering of survival signals that mediate phosphorylation of Bad found in Hepa1c1c7 cells. In contrast, despite a slight increase in p-Bad at 48 h, no increase in cell survival signals was seen in the F258 model, which may give additional explanations to the apparent high sensitivity of this cell line at low concentrations of B[*a*]P. Based on the metabolic studies, a possible explanation could be that the type of cyp enzyme was crucial for the resulting cell signaling. However, the lack of both survival signals as well as cyp induction in the F258 cells could also imply a role for the AhR receptor in the activation of cell survival signals. These suggestions as well as possible upstream events to the activations are important questions to be answered in order to justify *in vivo* extrapolations, and are currently under investigation.

In conclusion, B[*a*]P induces different cell signals and triggers clearly distinct apoptotic pathways in the two hepatic epithelial cell lines that apparently are not a result of the different experimental conditions used. The NHE1 pathway found to be important in B[*a*]P-induced apoptosis in F258 cells, seems to have no role in Hepa1c1c7 cells. While "classical" Bax translocation to the mitochondria resulting in cytochrome *c* release was important in Hepa1c1c7 cells, no such changes were seen in F258 cells. It is suggested that the rate of metabolism of B[*a*]P and type of reactive metabolites formed influence the resulting balance of pro-apoptotic and anti-apoptotic cell signaling, and hence the mechanisms involved in cell death and the chances of more permanent genetic damage.

Acknowledgements

The study has been supported by an Aurora grant (Egide) and Cancer Research, UK and the financial support is greatly appreciated. Volker M. Arlt is a member of the Environmental Cancer Risk, Nutrition and Individual Susceptibility (ECNIS) EU Network of Excellence. We thank Ingrid V. Botnen and Leni Ekeren for skilled technical assistance. We wish to thank the microscopy platform and Dr. Dutertre (UMR 6061, CNRS, Rennes) for helpful advice on immunolocalization captures and analyzes.

References

[1] IARC, Monographs on the evaluation of carcinogenic risk of chemicals to humans, in: Polynuclear Aromatic Compounds. Part 1. Chemical, Environmental and Experimental Data, IARC Sci. Publ., Lyon, France, 1983.
[2] European Center for Environment and Health, Organics, WHO, Bilthoven, The Netherlands, 1996.
[3] O. Hankinson, The aryl hydrocarbon receptor complex, Annu. Rev. Pharmacol. Toxicol. 35 (1995) 307–340.
[4] A. Dipple, Reactions of Polycyclic Aromatic Hydrocarbons with DNA, IARC Sci. Publ., 1994, pp. 107–129.
[5] E.L. Cavalieri, E.G. Rogan, Central role of radical cations in metabolic activation of polycyclic aromatic hydrocarbons, Xenobiotica London 25 (1995) 677–688.
[6] M. Reed, M. Monske, F. Lauer, S. Meserole, J. Born, S. Burchiel, Benzo[*a*]pyrene diones are produced by photochemical and enzy-

matic oxidation and induce concentration-dependent decreases in the proliferative state of human pulmonary epithelial cells, J. Toxicol. Environ. Health A 66 (2003) 1189–1205.
[7] J.H. Hoeijmakers, Genome maintenance mechanisms for preventing cancer, Nature 411 (2001) 366–374.
[8] W.P. Roos, B. Kaina, DNA damage-induced cell death by apoptosis, Trends Mol. Med. 12 (2006) 440–450.
[9] L. Henderson, A. Wolfreys, J. Fedyk, C. Bourner, S. Windebank, C.E. Ogburn, J. Oshima, M. Poot, R. Chen, K.E. Hunt, K.A. Gollahon, P.S. Rabinovitch, G.M. Martin, B. Kaina, S. Haas, H. Kappes, The ability of the Comet assay to discriminate between genotoxins and cytotoxins, Mutagenesis 13 (1998) 89–94.
[10] S.P. Hussain, C.C. Harris, p53 mutation spectrum and load: the generation of hypotheses linking the exposure of endogenous or exogenous carcinogens to human cancer, Mutat. Res. 428 (1999) 23–32.
[11] L.J. Hofseth, S.P. Hussain, C.C. Harris, p53: 25 years after its discovery, Trends Pharmacol. Sci. 25 (2004) 177–181.
[12] A. Solhaug, M. Refsnes, J.A. Holme, Role of cell signalling involved in induction of apoptosis by benzo[*a*]pyrene and cyclopenta[*c*,*d*]pyrene in Hepa1c1c7 cells, J. Cell. Biochem. 93 (2004) 1143–1154.
[13] A. Solhaug, M. Refsnes, M. Låg, P.E. Schwarze, T. Husoy, J.A. Holme, Polycyclic aromatic hydrocarbons induce both apoptotic and anti-apoptotic signals in Hepa1c1c7 cells, Carcinogenesis 25 (2004) 809–819.
[14] A. Solhaug, S. Ovrebo, S. Mollerup, M. Lag, P.E. Schwarze, S. Nesnow, J.A. Holme, Role of cell signaling in B[*a*]P-induced apoptosis: characterization of unspecific effects of cell signaling inhibitors and apoptotic effects of B[*a*]P metabolites, Chem. Biol. Interact. 151 (2005) 101–119.
[15] L. Huc, L. Sparfel, M. Rissel, M.T. Dimanche-Boitrel, A. Guillouzo, O. Fardel, D. Lagadic-Gossmann, Identification of Na^+/H^+ exchange as a new target for toxic polycyclic aromatic hydrocarbons, FASEB J. 18 (2004) 344–346.
[16] L. Huc, M. Rissel, A. Solhaug, X. Tekpli, M. Gorria, A. Torriglia, J.A. Holme, M.T. Dimanche-Boitrel, D. Lagadic-Gossmann, Multiple apoptotic pathways induced by p53-dependent acidification in benzo[*a*]pyrene-exposed hepatic F258 cells, J. Cell. Physiol. 208 (2006) 527–537.
[17] V.M. Arlt, H. Glatt, E. Muckel, U. Pabel, B.L. Sorg, H.H. Schmeiser, D.H. Phillips, Metabolic activation of the environmental contaminant 3-nitrobenzanthrone by human acetyltransferases and sulfotransferase, Carcinogenesis 23 (2002) 1937–1945.
[18] L. Payen, A. Courtois, S. Langouet, A. Guillouzo, O. Fardel, Unaltered expression of multidrug resistance transporters in polycyclic aromatic hydrocarbon-resistant rat liver cells, Toxicology 156 (2001) 109–117.
[19] R. Wiger, H.S. Finstad, J.K. Hongslo, K. Haug, J.A. Holme, Paracetamol inhibits cell cycling and induces apoptosis in HL-60 cells, Pharmacol. Toxicol. 81 (1997) 285–293.
[20] V.M. Arlt, H.H. Schmeiser, G.P. Pfeifer, Sequence-specific detection of aristolochic acid–DNA adducts in the human p53 gene by terminal transferase-dependent PCR, Carcinogenesis 22 (2001) 133–140.
[21] D.H. Phillips, M. Castegnaro, Standardization and validation of DNA adduct postlabelling methods: report of interlaboratory trials and production of recommended protocols, Mutagenesis 14 (1999) 301–315.
[22] D. Lagadic-Gossmann, M. Rissel, M. Galisteo, A. Guillouzo, Intracellular pH alterations induced by tacrine in a rat liver biliary epithelial cell line, Br. J. Pharmacol. 128 (1999) 1673–1682.
[23] L. Huc, D. Gilot, C. Gardyn, M. Rissel, M.T. Dimanche-Boitrel, A. Guillouzo, O. Fardel, D. Lagadic-Gossmann, Apoptotic mitochondrial dysfunction induced by benzo(*a*)pyrene in liver epithelial cells: role of p53 and pH_i changes, Ann. NY Acad. Sci. U.S.A. 1010 (2003) 167–170.
[24] K.J. Buckler, R.D. Vaughan-Jones, Application of a new pH-sensitive fluoroprobe (carboxy-SNARF-1) for intracellular pH measurement in small, isolated cells, Pflugers, Arch 417 (1990) 234–239.
[25] J.C. Gautier, S. Lecoeur, J. Cosme, A. Perret, P. Urban, P. Beaune, D. Pompon, Contribution of human cytochrome P450 to benzo[*a*]pyrene and benzo[*a*]pyrene-7,8-dihydrodiol metabolism, as predicted from heterologous expression in yeast, Pharmacogenetics 6 (1996) 489–499.
[26] E. Aklillu, S. Ovrebo, I.V. Botnen, C. Otter, M. Ingelman-Sundberg, Characterization of common CYP1B1 variants with different capacity for benzo[*a*]pyrene-7,8-dihydrodiol epoxide formation from benzo[*a*]pyrene, Cancer Res. 65 (2005) 5105–5111.
[27] S. Nesnow, C. Davis, G.B. Nelson, G. Lambert, W. Padgett, M. Pimentel, A.H. Tennant, A.D. Kligerman, J.A. Ross, Comparison of the genotoxic activities of the K-region dihydrodiol of benzo[*a*]pyrene with benzo[*a*]pyrene in mammalian cells: morphological cell transformation; DNA damage; and stable covalent DNA adducts, Mutat. Res. 521 (2002) 91–102.
[28] B. Beltran, M. Quintero, E. Garcia-Zaragoza, E. O'Connor, J.V. Esplugues, S. Moncada, Inhibition of mitochondrial respiration by endogenous nitric oxide: a critical step in Fas signaling, Proc. Natl. Acad. Sci. U.S.A. 99 (2002) 8892–8897.
[29] J.E. Ricci, R.A. Gottlieb, D.R. Green, Caspase-mediated loss of mitochondrial function and generation of reactive oxygen species during apoptosis, J. Cell. Biol. 160 (2003) 65–75.
[30] M.H. Harris, C.B. Thompson, The role of the Bcl-2 family in the regulation of outer mitochondrial membrane permeability, Cell Death Differ. 7 (2000) 1182–1191.
[31] S.B. Bratton, G.M. Cohen, Apoptotic death sensor: an organelle's alter ego? Trends Pharmacol. Sci. 22 (2001) 306–315.
[32] D.W. Meek, The p53 response to DNA damage, DNA Repair (Amst.) 3 (2004) 1049–1056.
[33] T. Unger, R.V. Sionov, E. Moallem, C.L. Yee, P.M. Howley, M. Oren, Y. Haupt, Mutations in serines 15 and 20 of human p53 impair its apoptotic activity, Oncogene 18 (1999) 3205–3212.
[34] J. Zha, H. Harada, E. Yang, J. Jockel, S.J. Korsmeyer, Serine phosphorylation of death agonist BAD in response to survival factor results in binding to 14-3-3 not BCL-X(L), Cell 87 (1996) 619–628.
[35] J.M. Lizcano, N. Morrice, P. Cohen, Regulation of BAD by cAMP-dependent protein kinase is mediated via phosphorylation of a novel site, Ser155, Biochem. J. 349 (2000) 547–557.
[36] S.R. Datta, H. Dudek, X. Tao, S. Masters, H. Fu, Y. Gotoh, M.E. Greenberg, Akt phosphorylation of BAD couples survival signals to the cell-intrinsic death machinery, Cell 91 (1997) 231–241.
[37] X. Fang, S. Yu, A. Eder, M. Mao, R.C. Bast Jr., D. Boyd, G.B. Mills, Regulation of BAD phosphorylation at serine 112 by the Ras-mitogen-activated protein kinase pathway, Oncogene 18 (1999) 6635–6640.